Progress In Electromagnetics Research, Vol. 131, 293–310, 2012

DESIGN AND IMPLEMENTATION OF AN ULTRA-WIDEBAND SIX-PORT NETWORK

H. Peng*, Z. Q. Yang, and T. Yang

School of Electronic Engineering, University of Electronic Science and Technology of China, Chengdu, Sichuan 611731, China

Abstract—This paper presents a six-port network over an ultra-wideband (UWB) of 2–8 GHz. Its key component is the six-port junction, which consists of a Wilkinson power divider and three 3-dB quadrature couplers. This six-port junction is accomplished in a low dielectric constant substrate (Rogers RT/duroid 5880). Multi-section impedance transformation is applied in the power divider, and the quadrature coupler is realized by using two 8.34 dB couplers in tandem. An ultra-wideband operation of the six-port junction is verified by full electromagnetic simulations and measurements. The results show that the designed devices exhibit good performance across 2–8 GHz band: the return losses at input ports are higher than 15 dB, the insertion losses from input ports to the remaining ports are 7.2 dB ± 1.7 dB, the isolation between two input ports is greater than 20.5 dB, and the maximum phase difference compared with the theoretical behavior between two test ports is 10°. For the manufactured six-port junction, a six-port phase measurement system and a calibration technique based on support vector regression (SVR) are introduced. Results show that the SVR model can achieve a mean phase error of 1.5274°.

1. INTRODUCTION

An earlier research of the six-port technique was proposed in 1972 by Hoer [1]. The six-port technique was demonstrated to be a suitable option as the ratio of complex amplitude measurements in [2–4]. Many microwave applications directly or indirectly require the determination of phase differences between two input microwave signals over a specified frequency band, such as microwave vector network analyzers (VNA) [5], direction finding [6, 7], position sensors [8],

Received 6 July 2012, Accepted 27 August 2012, Scheduled 14 September 2012

* Corresponding author: Hao Peng (ph1984.1.25@163.com).

frequency measurement [9], digital signal demodulation [10], and other applications [11–16]. The six-port technique adopts a zero-intermediate frequency architecture, whose advantages are listed: no mixer, no image frequency, high integrated level, low cost, reconfigurability, etc. Furthermore, the six-port network has an extremely wide bandwidth, and can provide multi-standard capabilities. It is a particularly suitable application in MMIC [17].

The key component of the six-port technique is the six-port junction, which consists of a power divider and three 3-dB quadrature couplers. The performance of the six-port junction has a direct impact on the indicators of the system, such as phase accuracy for VNA, determination of beam direction angle, distance estimation, frequency accuracy, bit error ratio (BER), etc. It is researchers' goal to design a six-port junction as close as possible to the theoretical situation in a wider bandwidth.

In this paper, a six-port junction, over the ultra-wideband (UWB) of 2–8 GHz, is presented. The six-port junction is accomplished in a low dielectric constant substrate (Rogers 5880). A 3-dB coupler can also be realized by adopting two 8.34-dB couplers in tandem. A conventional Wilkinson power divider is applied in our design. To compensate the phase deviation originating in the via, a short stripline is added into the circuit.

Based on the manufactured six-port junction, a six-port phase measurement system is built. This system consists of a six-port junction, a phase shifter, the operation amplifiers, four detectors, a power divider, and other devices. The nonlinearity of diode detectors and the asymmetry of six-port junctions can inevitably cause phase errors. Therefore, a calibration technique is employed to improve the performance of the measurement phase.

In this paper, a calibration technique based on support vector regression (SVR) is proposed. Support vector machine (SVM) theory was advanced by Vapnik in 1995 [18], which has been successfully applied in regression problems [19, 20]. SVM, based on the smallsample statistical learning theory embodies the structural risk minimization (SRM) principle, and can solve a constrained quadratic optimization problem Therefore, SVM can always find a global minimum.

The rest of the paper is organized as follows. In Section 2, the design principle of the six-port junction is discussed. In Section 3, an example is given to demonstrate the design principle, a phase measurement system is introduced, and a calibration technique based on the SVR is presented. And the finally Section goes to the conclusion of this paper.

2. CICUIT DESIGN

The principle of a six-port junction for an ultra-wideband application is discussed in this section. Figure 1 shows the structure of the six-port junction. It consists of a power divider and three 3-dB quadrature couplers [21].

2.1. Power Divider

In previous studies, various types of power dividers have been presented [22–25]. Chebyshev four-section impedance transformation is used in a Wilkinson power divider. The relevant design theory and method can be found in the literature [26]. A Rogers RT/duroid 5880 substrate with a dielectric constant of 2.2, a loss tangent of 0.0009, a thickness of 0.787-mm, plus 17-µm-thick conductive coating is selected for the power divider development. For the center frequency 5 GHz, a quarter of the effective wavelength is equal to 10.91 mm. The microstrip lines forming the input/output ports of the coupler are designed to have 50 Ω-characteristic impedance ($W = 2.4$ mm). The configuration of an UWB power divider is shown in Figure 2, and the actual parameters of each section are listed in Table 1.

The simulated results of the power divider show that good performance is achieved over the entire bandwidth: the return loss

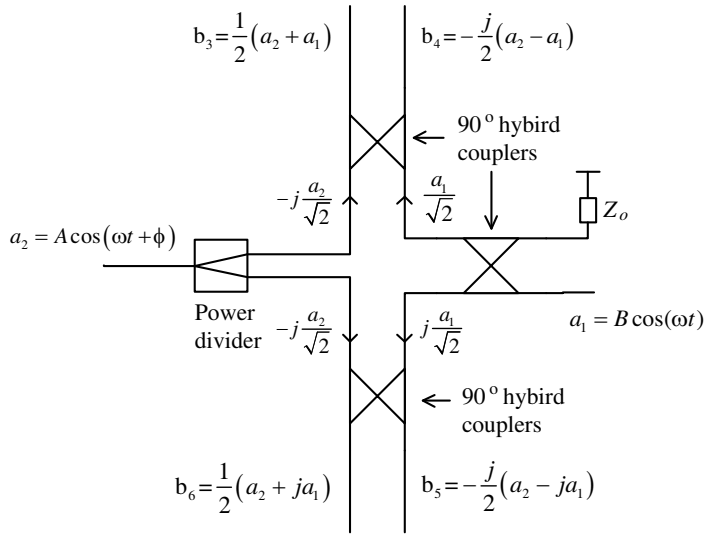

Figure 1. Six-port junction topology.

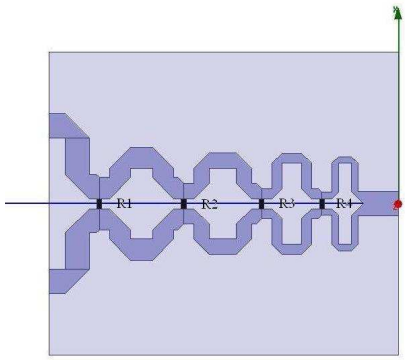

Figure 2. Layout of Wilkinson power divider.

Table 1. Parameters of each section and isolation resistance.

Sections: $N = 4$	$n = 1$	$n = 2$	$n = 3$	$n = 4$
Impedance: Z_n (Ω)	54.55	66.17	83.31	101.1
Width: W_n (mm)	2.1	1.53	1	0.66
Isolation R: R_n (Ω)	430	360	200	100

of each port is higher than 20.1 dB, the insertion losses between input and output ports are better than 3.32 dB, the amplitude imbalance is less than 0.15 dB, the phase imbalance is less than 0.25°, and the isolation between two output ports is higher than 23.2 dB.

2.2. 3-dB Quadrature Coupler

In previous studies, various types of 3-dB quadrature couplers have been presented [27–33]. However, these couplers are inherently narrowband circuits (less than one octave). A tight coupler can be realized by adopting two weak couplers in tandem. For example, a 3-dB quadrature coupler can be realized from the tandem connection of two 8.34-dB multisection couplers [34–36]. Consequently, a 3-dB coupler, composed of two identical 8.34-dB seven-section couplers with broadside-coupled striplines, is developed using a Rogers RT/duroid 5880 substrate with a dielectric constant of 2.2 and a dielectric loss tangent of 0.0009, plus 17-μm-thick conductive coating. The structure is formed like a 0.787 mm–0.254 mm–0.787 mm sandwich, and printed metal lines are arranged on the top and bottom side of the central layer with the decrease of alignment errors. Figure 3 shows the configuration of 3-dB quadrature coupler, and Table 2 lists the actual parameters of

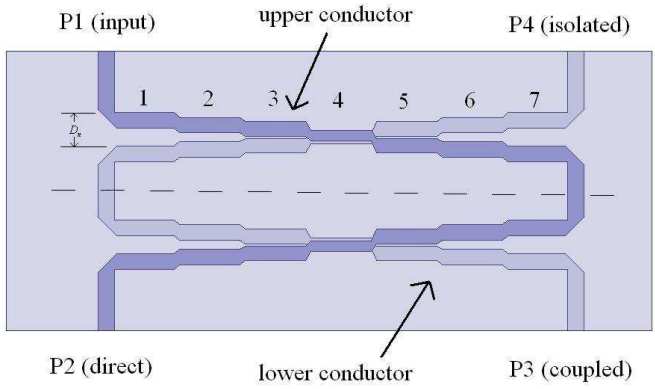

Figure 3. Layout of 3-dB quadrature coupler.

Table 2. Parameters of each section.

Sections: $N = 4$	$n = 1$	$n = 2$	$n = 3$	$n = 4$	$n = 5$	$n = 6$	$n = 7$
Even mode impedance: Z_{en} (Ω)	50.17	52.48	59.67	98.28	59.67	52.48	50.17
Odd mode impedance: Z_{on} (Ω)	48.85	46.65	41.16	24.93	41.16	46.65	48.85
Width: W_n (mm)	1.45	1.44	1.35	0.95	1.35	1.44	1.45
Offset distance: D_n (mm)	3.14	2.28	1.57	0.28	1.57	2.28	3.14

each section of a 8.34-dB multisection coupler.

The simulated results of the 3-dB quadrature coupler show that good performance is achieved over the entire bandwidth: the return loss of each port is higher than 19.1 dB, the insertion losses between the input port and two output ports are better than 3.45 dB, the amplitude imbalance is less than 0.44 dB, the phase imbalance is less than 1.3°, and the isolation between the input port and isolated port is higher than 19.5 dB.

2.3. Six-port Junction

Figure 1 shows the principle of the six-port junction. The structures of the power divider and coupler, mentioned in Sections 2.1 and 2.2, are employed to constitute the six-port junction. Figure 4 shows the configuration of the six-port junction. The dark part is the upper conductor, and the light part is the lower conductor. As for the six-port junction, two problems need to be solved: 1) the transition of the microstrip line and stripline; 2) the compensation of phase deviation originating in the via.

A four-section Wilkinson power divider is realized on a microstrip line substrate, and the coupler is achieved in a stripline substrate. The characteristic impedances of the microstrip line forming the output ports and the stripline forming the input ports are both $50\,\Omega$. Consequently, two types of circuits for signal transmission can be directly connected. Because of the bifacial structure of the 3-dB quadrature coupler, the upper stripline has to be connected to the lower stripline by a via for the central layer. During this process, a discontinuity in microstrip line can affect the circuit performance, and the via could also cause the phase deviation. A compensation method, shown in Figure 5, is that a short stripline is added into the circuit to imitate the influence of the via. Simulation results show that, due to the added short stripline ($l_2 - l_1 = 0.12\,\text{mm}$), the errors are reduced from $2.7°$ ($l_2 = l_1$) to only $0.43°$.

$S_{\Delta i1}$ and $S_{\Delta i2}$ are firstly defined as follows:

$$S_{\Delta i1} = phase(S_{i1}) - phase(S_{41}) \quad (i = 3, 4, 5, 6) \tag{1}$$

$$S_{\Delta i2} = phase(S_{i2}) - phase(S_{42}) \quad (i = 3, 4, 5, 6) \tag{2}$$

The simulated results of the six-port junction present good performance over the entire bandwidth: the return loss of each port

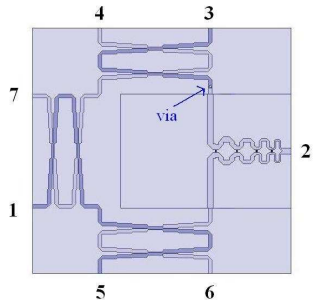

Figure 4. Layout of six-port junction.

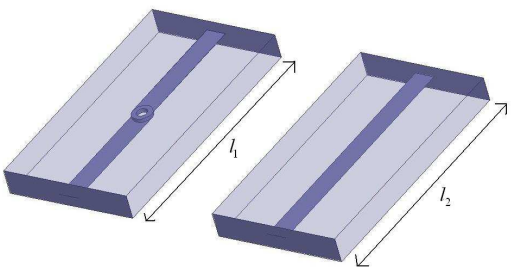

Figure 5. Compensation schematic of the via.

is higher than 15.5 dB, the insertion losses from port 1 or 2 to the remaining ports are 6.68 ± 1.18 dB, the isolation between ports 1 and 2 is higher than 23.8 dB. Compared with the theoretical behavior, the maximum phase difference of $S_{\Delta i1}$ and $S_{\Delta i2}$ are 2.3° and 5.7° respectively.

3. RESULTS

This section aims to analyse the simulated and measured results of the proposed six-port junction, and the phase errors of the six-port microwave measurement system over the entire bandwidth. S-parameters of six-port junction are measured by the Agilent E8363B network analyzer. In order to obtain the phase errors of the system, four detectors, a power divider, an operation amplifier, a phase shifter, and other devices are added. The microwave pulse signal is generated by Agilent synthesized sweeper E8257, and the pulse voltages of the I/Q signals can be directly displayed on the digital oscilloscope.

3.1. Results of the Six-port Junction

A photograph of the manufactured six-port is shown in Figure 6. Note that port 7 is connected to a matched load.

In the ideal case, the six-port junction should feature high return losses at ports 1 and 2, high isolation between ports 1 and 2, and 6-dB insertion losses from ports 1 and 2 to ports 3–6. Figure 7 shows both the simulated and measured results of return and insertion losses of the six-port.

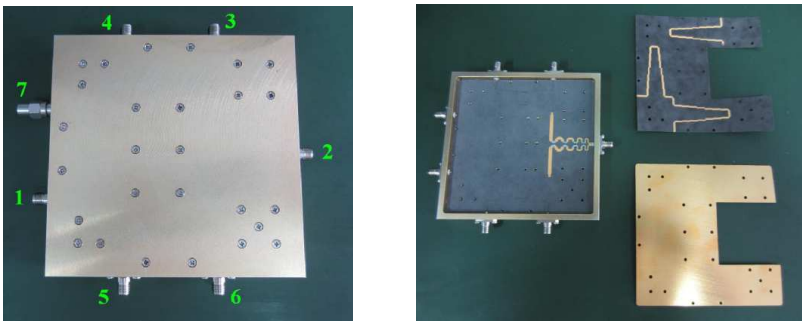

(a) (b)

Figure 6. Photograph of the manufactured six-port junction: (a) External appearance; (b) Internal composition.

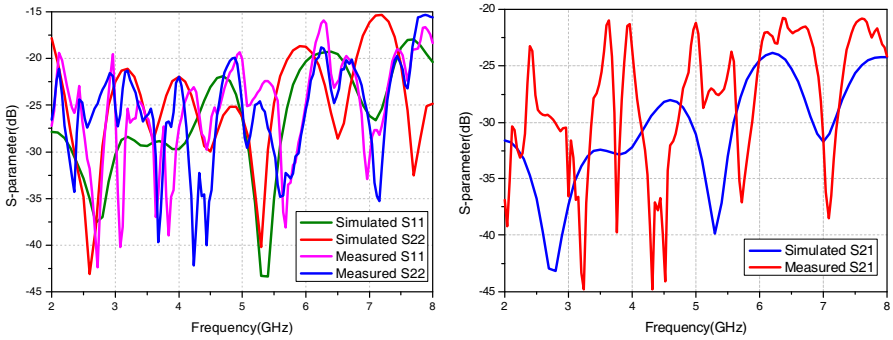

Figure 7. Results: (a) Simulated and measured input return loss at ports 1 and 2; (b) Isolation between port 1 and 2.

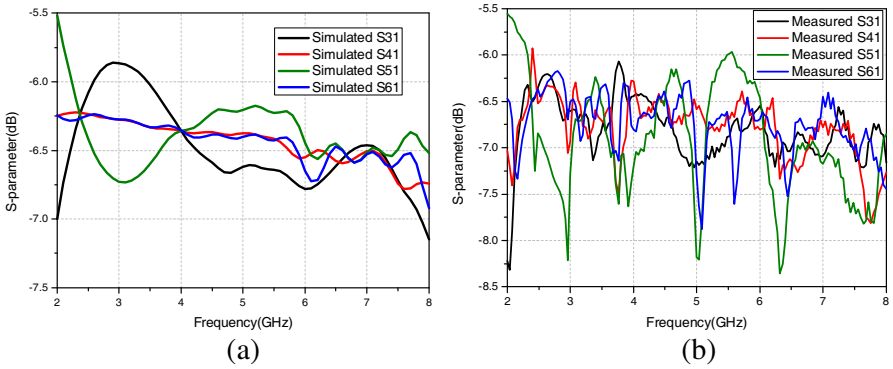

Figure 8. Results: (a) Simulated insertion losses from port 1 to the remaining ports; (b) Measured insertion losses from port 1 to the remaining ports.

Figure 8 shows both the simulated and measured results of insertion losses from port 1 to the remaining ports.

Figure 9 shows both the simulated and measured results of insertion losses from port 2 to the remaining ports.

The following content is related to the phase characteristics of the six-port junction. For the phase of transmission coefficients between port 1 or port 2 and the remaining ports, it is important to approximately maintain a constant unrelated to the operation frequency of a chosen reference port. For the ideal case, the constant should be an integer multiple of 90°. Figure 10 shows the absolute phase of S_{41} and S_{42}.

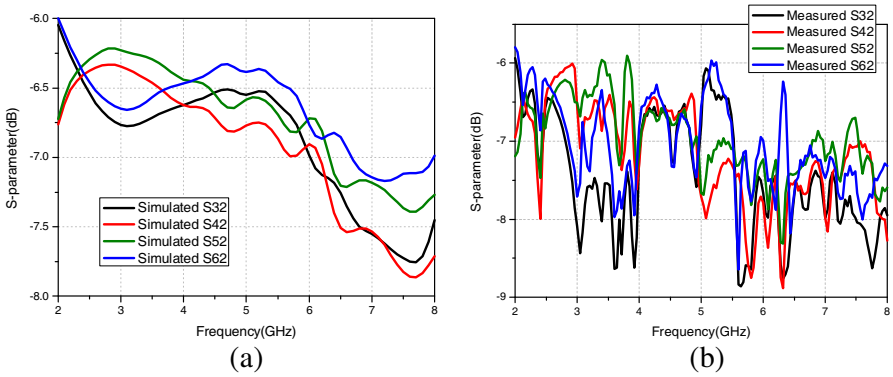

Figure 9. Results: (a) Simulated insertion losses from port 2 to the remaining ports; (b) Measured insertion losses from port 2 to the remaining ports.

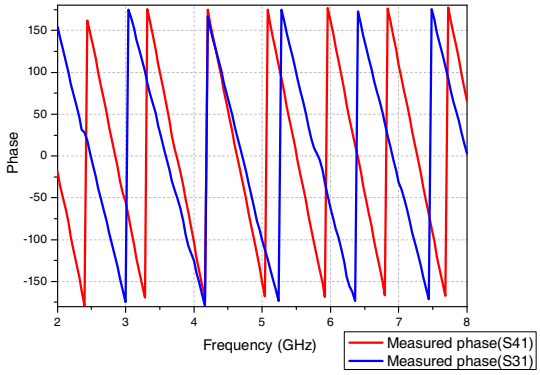

Figure 10. Absolute phase of S_{41} and S_{31}.

As Figure 11 shown, all of the remaining phases are referenced against phase (S_{41}) or phase (S_{31}).

The measured results of the six-port junction show good performance over the entire bandwidth: the return loss of each port is higher than 15 dB, the insertion losses from port 1 or 2 to the remaining ports are 7.2 ± 1.7 dB, and the isolation between ports 1 and 2 is higher than 20.5 dB. The maximum phase difference of $S_{\Delta i1}$ or $S_{\Delta i2}$ are all 10° compared with the theoretical behavior.

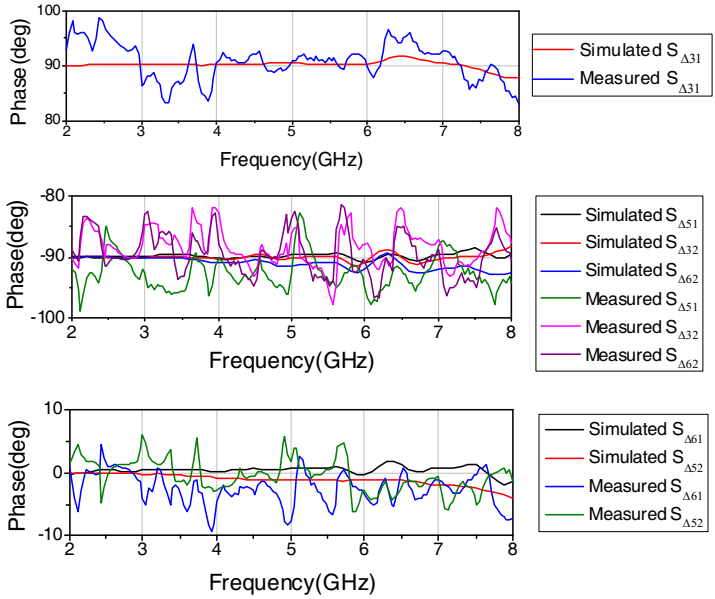

Figure 11. Simulated and measured phase response.

3.2. Phase Errors of Six-port Microwave Measurement System

The six-port microwave measurement system, essentially based on the phase measurement system, must combine the six-port junction with other components, such as power detectors, differential amplifiers and a signal processor. The phase errors are the main concern of our research. Figure 12 shows the block diagram of the six-port phase measurement system. The power detectors are required to operate in a square law range. Figure 13 shows a photograph of the test platform, including a six-port junction, a phase shifter, operation amplifiers, four detectors, a power divider, and other devices.

In the ideal case, the phase differences of two signals can be calculated by using the I/Q amplitudes, and be expressed as follows [21]:

$$V_n = \frac{K}{4}\left[A^2 + B^2 + 2\cdot(-1)^n \cdot A \cdot B \cdot \cos\left(\phi + j\cdot\pi/2\right)\right] \quad \begin{cases} j = 0, & \text{if } n = 3,4 \\ j = -1, & \text{if } n = 5,6 \end{cases} \tag{3}$$

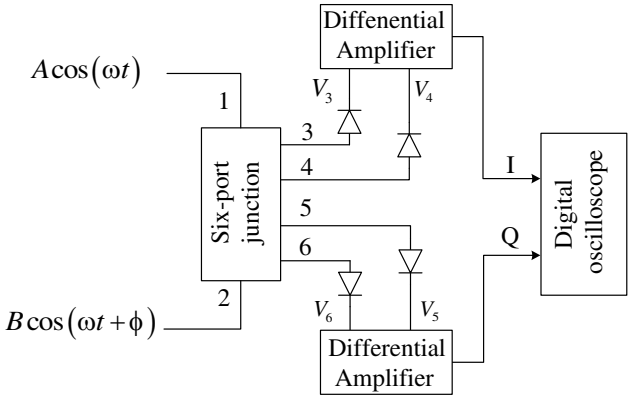

Figure 12. Six-port phase measurement system.

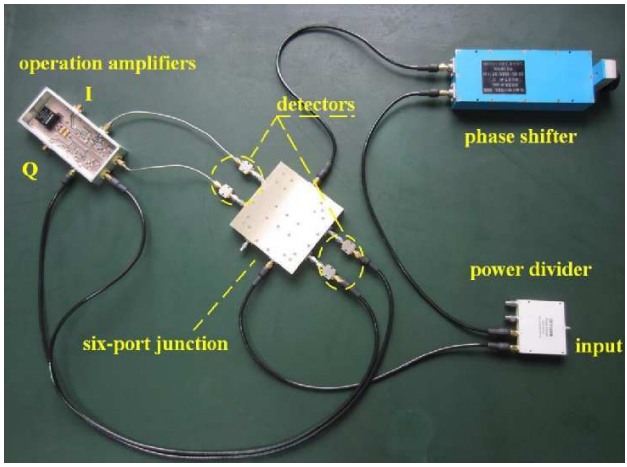

Figure 13. Test platform.

$$\phi = \tan^{-1}\left(\frac{V_6 - V_5}{V_4 - V_3}\right) \tag{4}$$

where V_n is the ideal output voltage of the detector; K is the constant factor; A and B denote the amplitudes of the input signals of the six-port network; n is the correlator output port index; and ϕ represents the phase difference between the injected signals of the six-port network.

Considering the nonlinearity of the diode detectors and the asymmetry of the six-port junction, Equation (3) can be rewritten

as:

$$V'_n = K_n\Big\{(A\cdot|S_{n1}|)^2+(B\cdot|S_{n2}|)^2+2\cdot A\cdot B\cdot|S_{n1}|\,|S_{n2}| \cdot\cos\left[phase\left(S_{41}\right)+S_{\Delta n1}-\phi-phase\left(S_{42}\right)-S_{\Delta n2}\right]\Big\} \quad (n=3,\ 4,\ 5,\ 6) \tag{5}$$

where V'_n is the actual output voltage of the detector and K_n the conversion factor of the diode detector between power and voltage. Note that K_n is a function of input power and frequency. It is difficult to acquire the exact values of V'_n via Equation (5). The initial phase of $phase\left(S_{41}\right)-phase\left(S_{42}\right)$ can be measured by the vector network analyzer, and it is only a function of frequency as a known quantity. The operation frequency of system may be a known condition or can be obtained by frequency measurement technology [7]. The calculated phase ϕ' can be expressed as:

$$\phi' = \tan^{-1}\left(\frac{V'_6-V'_5}{V'_4-V'_3}\right)+phase\left(S_{41}\right)-phase\left(S_{42}\right) \tag{6}$$

The calculated phase ϕ' changes along with the change of the input phase difference ϕ. The values of $\phi'-\phi$ are defined as the phase errors and recorded. The input phase differences ϕ are set as 0° to 360° at 10° intervals, and the frequencies are set as 2 to 8 GHz at 500 MHz intervals. Compared with the theoretical behavior, the maximum phase difference are all 10° for $S_{\Delta i1}$ or $S_{\Delta i2}$. However, as shown in Figure 14, most of the maximum phase errors for test frequencies are better than ±20°. The differences between them are mainly due to the nonlinearity and asymmetry of the diode detectors, and the asymmetry of the operation amplifiers.

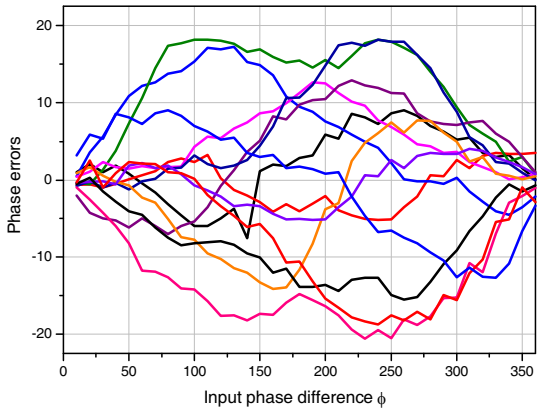

Figure 14. Phase errors of six-port microwave measurement system.

3.3. Calibration of the Six-port Network

This six-port network can be directly used in digital communication without a calibration technique, such as QPSK and BPSK. However, different modulation schemes and various application situations would also be taken into the consideration for the phase accuracy, which can't meet these requirements. Therefore, a calibration technique based on the SVR is introduced.

The SVM, which embodies the SRM principle, is a small-sample statistical learning machine. In theory, this method always identifies global minima. The LIBSVM toolbox, developed by Chang and Lin, is utilized to calculate the various models [37]. The SVR parameters could be determined before running code: the constant definition of kernel function (γ), tolerance of termination criterion (ε), penalty parameter (C), and constant ν. $\nu \in [0, 1]$ is the parameter that controls the number of support vectors. The K-fold cross-validation method is used to calculate the optimal parameters of γ and C. The SVR parameters are as follows: $\varepsilon = 0.0001$, $\nu = 0.1$, $C = 4$ and $\gamma = 1$. The Root Mean Square Error ($RMSE$) and Pearson Product-Moment correlation coefficient (R) are calculated to determine the accuracy of the SVR model. $RMSE$ and R are expressed as:

$$RMSE = \sqrt{\frac{1}{N}\sum_{i=1}^{N}(a_i - b_i)^2} \tag{7}$$

$$R = \frac{\sum_{i=1}^{N}\left(b_i - \bar{b}\right)(a_i - \bar{a})}{\sqrt{\sum_{i=1}^{N}\left(b_i - \bar{b}\right)^2 \sum_{i=1}^{N}(a_i - \bar{a})^2}} \tag{8}$$

where a_i is the predicted phase difference of the training or cross-validation data set based on the SVR model, $\bar{a}$ the mean of the predicted phase difference of the training or cross-validation data set, b_i the real phase difference, $\bar{b}$ the mean of the real phase difference, and N the data number.

The operation frequency of the system may be a known condition or can be obtained by frequency measurement technology [7]. The initial phase of $phase\,(S_{41}) - phase\,(S_{42})$ can be measured by the vector network analyzer, and it is only a function of frequency as a known quantity. For simplicity, the calibration technique of the six-port network is only considered at a fixed frequency in this paper. The input phase difference is set as 0° to 315.6° at 1.2° intervals at 5 GHz.

Table 3. RMSE and R of the training and cross-validation data sets.

	Training Data Set (200 samples)	Cross-Validation Data Set (64 samples)
$RMSE$	1.4067°	1.5274°
R	0.9999	0.9998

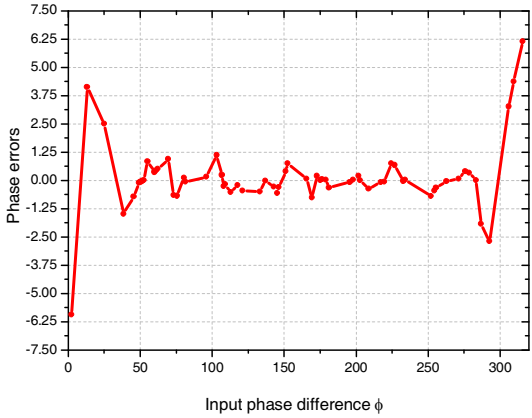

Figure 15. Phase errors statistics.

A total of 264 standards are established, and all readings (I, Q) are measured and recorded. 75% of the data (200 samples) are randomly selected as the training data set, and the rest are classified as the cross-validation data set (64 samples).

For the training data set, the $RMSE$ of the phase error is 1.4067°. The fresh cross-validation data set (64 samples) is used to determine the accuracy of the proposed SVR model. For the cross-validation data set, the $RMSE$ is 1.5274°. These results are summarized in Table 3, which indicates that the SVR model predicts the results well.

Figure 15 shows that the phase errors (°) of most of the predicted results are less than ±1.25°. The performance of the six-port network, based on the calibration technique, is advanced greatly.

4. CONCLUSION

In this paper, an ultra-wideband six-port junction from 2 to 8 GHz is presented, which is part of a phase measurement system. Its UWB operation has been verified by both simulation and measurement. The designed devices have been manufactured, showing good experimental

performance during the test. Based on the calibration technique, the SVR model can achieve a mean phase error of 1.5274°, which means that the phase errors of most of the predicted results are less than ±1.25°. In a word, this ultra-wideband six-port network is a promising candidate for digital communication, microwave measurement, software defined radio (SDR), and other applications.

ACKNOWLEDGMENT

This work was supported by the National Natural Science Foundation of China (Grant No. 61006026).

REFERENCES

1. Hoer, C. A., "The six-port coupler: A new approach to measuring voltage, current, power, impedance and phase," *IEEE Trans. Instrum. Meas.*, Vol. 21, No. 4, 466–470, Nov. 1972.
2. Cicolani, M. and F. Marchetti, "Phase and amplitude automatic measurements on pulsed RF signals," *Twenty-second European Microwave Conference*, Helsinki, Finland, Sep. 1992.
3. Galwas, B. and S. Palczewski, "Idea of six-port vector-voltmeter with homodyne phase-sensitive detectors," *Ninth Instrumentation and Measurement Technology Conference*, New York, United States, 1992.
4. Galwas, B. and S. Palczewski, "Broadband homodyne six-port reflectometer," *Proc. 21st European Microwave Conference*, Stuttgart, Germany, 1991.
5. Engen, G. F., "The six-port reflectometer: An alternative network analyzer," *IEEE Trans. Microw. Theory Tech.*, Vol. 25, No. 12, 1075–1080, Dec. 1977.
6. Peng, H., T. Yang, and Z. Yang, "Calibration of a six-port position sensor via support vector regression," *Progress In Electromagnetics Research C*, Vol. 26, 71–81, 2012.
7. Peng, H., Z. Yang, and T. Yang, "Design and implementation of a practical direction finding receiver," *Progress In Electromagnetics Research Letters*, Vol. 32, 157–167, 2012.
8. Yang, J.-R. and S. Hong, "A Distance-compensated radar sensor with a six-port network for remote distinction of objects with different dielectric constants," *Journal of Electromagnetic Waves and Applications*, Vol. 24, Nos. 11–12, 1429–1437, 2010.
9. Coupez, J. P., H. Gruchala, A. Slowik, C. Recko, and A. Rutkowski, "High resolution IFMs," *14th International*

Conference on Microwaves, Radar and Wireless Communications, 2002, MIKON-2002, Gdańsk, Poland, 2002.

10. Khaddaj Mallat, N., E. Moldovan, and S. O. Tatu, "Comparative demodulation results for six-port and conventional 60 GHz direct conversion receivers," *Progress In Electromagnetics Research*, Vol. 84, 437–449, 2008.
11. Boukari, B., E. Moldovan, S. Affes, K. Wu, R. G. Bosisio, and S. O. Tatu, "A heterodyne six-port FMCW radar sensor architecture based on beat signal phase slope techniques," *Progress In Electromagnetics Research*, Vol. 93, 307–322, 2009.
12. De la Morena-Álvarez-Palencia, C. and M. Burgos-Garcia, "Four-octave six-port receiver and its calibration for broadband communications and software defined radios," *Progress In Electromagnetics Research*, Vol. 116, 1–21, 2011.
13. Moscoso-Martir, A., I. Molina-Fernandez, and A. Ortega-Monux, "Signal constellation distortion and BER degradation due to hardware impairments in six-port receivers with analog I/Q generation," *Progress In Electromagnetics Research*, Vol. 121, 225–247, 2011.
14. Hammou, D., E. Moldovan, and S. O. Tatu, "Modeling and analysis of a modified V-band MHMIC six-port circuit," *Journal of Electromagnetic Waves and Applications*, Vol. 24, No. 10, 1419–1427, 2010.
15. Moldovan, E., S. O. Tatu, T. Gaman, K. Wu, and R. G. Bosisio, "A new 94 GHz six port collision avoidance radar sensor," *IEEE Trans. Microw. Theory Tech.*, Vol. 52, No. 3, 751–759, Mar. 2004.
16. Xiao, F. C., F. M. Ghannouchi, and T. Yakabe, "Application of a six-port wave-correlator for a very low velocity measurement using the Doppler effect," *IEEE Trans. Instrum Meas.*, Vol. 52, No. 2, 297–301, Apr. 2003.
17. Tatu, S. O., E. Moldovan, G. Brehm, K. Wu, and R. G. Bosisio, "Ka-band direct digital receiver," *IEEE Trans. Microw. Theory Tech.*, Vol. 50, No. 11, 2436–2442, Nov. 2002.
18. Vapnik, V., *The Nature of Statistical Learning Theory*, Springer-Verlag, New York, 1995.
19. Xia, L., R. Xu, and B. Yan, "LTCC interconnect modeling by support vector regression," *Progress In Electromagnetics Research*, Vol. 69, 67–75, 2007.
20. Yang, Z. Q., T. Yang, Y. Liu, and S. H. Han, "MIM capacitor modeling by support vector regression," *Journal of Electromagnetic Waves and Applications*, Vol. 22, No. 1, 61–67,

2008.

21. Tatu, S. O., E. Moldovan, K. Wu, R. G. Bosisio, and T. A. Denidni, "Ka-band analog front-end for software-defined direct conversion receiver," *IEEE Trans. Microw. Theory Tech.*, Vol. 53, 2768–2776, Sep. 2005.
22. Lin, Z. and Q.-X. Chu, "A novel approach to the design of dual-band power divider with variable power dividing ratio based on coupled-lines," *Progress In Electromagnetics Research*, Vol. 103, 271–284, 2010.
23. Chiang, C. T. and B.-K. Chung, "Ultra wideband power divider using tapered line," *Progress In Electromagnetics Research*, Vol. 106, 61–73, 2010.
24. Wang, D., H. Zhang, T. Xu, H. Wang, and G. Zhang, "Design and optimization of equal split broadband microstrip Wilkinson power divider using enhanced particle swarm optimization algorithm," *Progress In Electromagnetics Research*, Vol. 118, 321–334, 2011.
25. Zhang, H., X.-W. Shi, F. Wei, and L. Xu, "Compact wideband Gysel power divider with arbitrary power division based on patch type structure," *Progress In Electromagnetics Research*, Vol. 119, 395–406, 2011.
26. Matthaei, G. L., L. Young, and E. M. T. Jones, *Microwave Filters Impedance-matching Networks, and Coupling Structures*, Artech House Books, Dedham, Mass, 1980.
27. Wong, Y. S., S. Y. Zheng, and W. S. Chan, "Multifolded bandwidth branch line coupler with filtering characteristic using coupled port feeding," *Progress In Electromagnetics Research*, Vol. 118, 17–35, 2011.
28. Sharma, R. Y., T. Chakravarty, S. Bhooshan, and A. B. Bhattacharyya, "Design of a novel 3 dB microstrip backward wave coupler using defected ground structure," *Progress In Electromagnetics Research*, Vol. 65, 261–273, 2006.
29. Shie, C.-I., J.-C. Cheng, S.-C. Chou, and Y.-C. Chiang, "Design of cmos quadrature vco using on-chip trans-directional couplers," *Progress In Electromagnetics Research*, Vol. 106, 91–106, 2010.
30. Liu, G.-Q., L.-S. Wu, and W.-Y. Yin, "A compact microstrip rat-race coupler with modified lange and T-shaped arms," *Progress In Electromagnetics Research*, Vol. 115, 509–523, 2011.
31. Wong, Y. S., S. Y. Zheng, and W. S. Chan, "Multifolded bandwidth branch line coupler with filtering characteristic using coupled port feeding," *Progress In Electromagnetics Research*, Vol. 118, 17–35, 2011.

32. Lange, J., "Interdigitated stripline quadrature hybrid," *IEEE Trans. Microw. Theory Tech.,* Vol. 17, No. 12, 1150–1151, Dec. 1969.
33. Cho, J.-H., H.-Y. Hwang, and S.-W. Yun, "A design of wideband 3-dB coupler with N-section microstrip tandem structure," *IEEE Microw. Wireless Compon. Lett.*, Vol. 15, No. 2, 113–115, Feb. 2005.
34. Shelton, J. P. and J. A. Mosko, "Synthesis and design of wide-band equal-ripple TEM directional couplers and fixed phase shifters," *IEEE Trans. Microw. Theory Tech.,* Vol. 14, No. 10, 462–473, Oct. 1966.
35. Carpenter, E., "The virtues of mixing tandem and cascade coupler connections," *1971 IEEE GMTT International Microwave Symposium Digest*, 8–9, 1971.
36. Walker, J. L. B., "Analysis and design of Kemp-type 3-dB quadrature couplers," *IEEE Trans. Microw. Theory Tech.*, Vol. 38, No. 1, 88–90, Jan. 1990.
37. Chang, C. C. and C. J. Lin, "LIBSVM: A library for support vector machines," System Documentation, National Taiwan University, 2004.